Inference of thermospheric temperature profiles from ultra-violet emission observations with the NASA *Global-scale Observations of the Limb and Disk* (GOLD) mission

Clayton Cantrall, Tomoko Matsuo – Department of Aerospace Engineering Sciences, University of Colorado – Boulder
CEDAR Workshop, Sante Fe, June 2018

Overview

Global monitoring of thermospheric state variables is currently non-existent, but inference of temperature profiles from the NASA Global Observations of Limb and Disk (GOLD) instrument offers the key to addressing a number of outstanding questions about how the Earth's upper atmosphere responds to tropospheric weather and space weather forcing.

GOLD provides an unprecedented global, high-cadence view of Earth's thermosphere in the far ultra-violet (UV) spectrum. A primary emission feature in the GOLD bandwidth is the Lyman-Birge-Hopfield (LBH) band emission caused by photo-electron impact excitation of N_2. The broadening of individual emission features within the LBH band, each feature corresponding to different vibrational transitions of N_2, provides information into the neutral temperature of the thermosphere.

Using the sensitivity of the LBH band to temperature, an inferential problem of the thermospheric temperature profiles from GOLD measurements can be formulated in a similar fashion to tropospheric radiance data assimilation approaches. The evaluation of our inference approaches has been conducted by using observing system simulation experiments with a nature run and 80-member ensemble simulations provided by the NOAA's whole atmosphere model (WAM) (Akmaev, 2011) and NCAR's airglow model (GLOW) and GOLD line-of-sight model (LOS) (Solomon, 2017).

Observations and Scientific Background

The GOLD instrument is an imaging spectrograph that measures UV airglow emissions between 132-162 nm with a resolution of 0.2-2.2 nm. The high spectral resolution of GOLD provides an opportunity to retrieve the neutral temperature of the thermosphere through the broadening of LBH emission features (Aksnes et al. 2006).

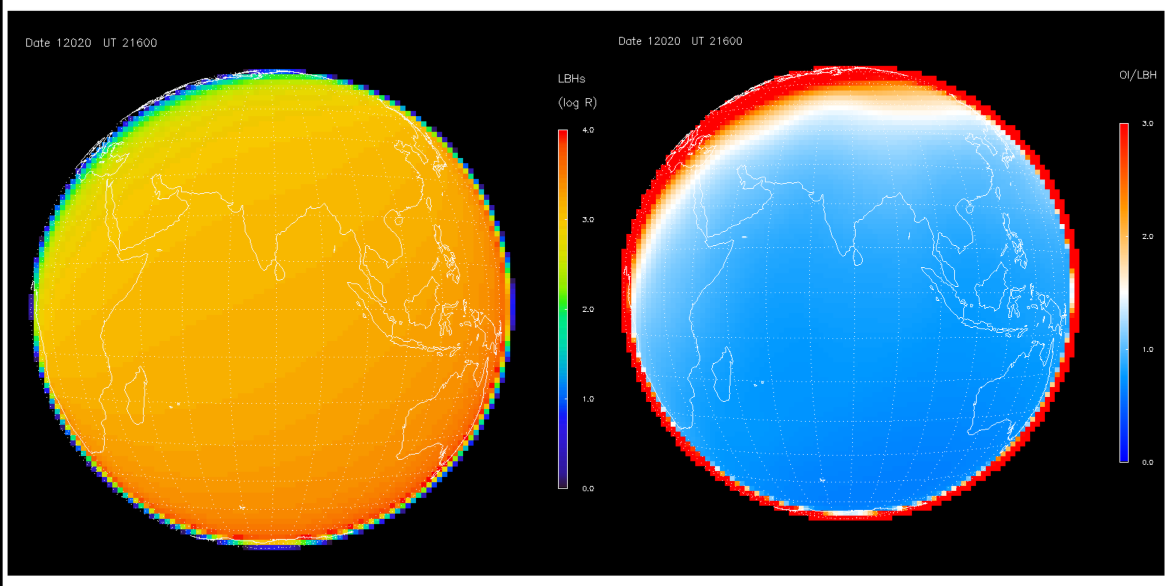

Figure 1: Synthetic GOLD observations of LBH and O/LBH ratio emissions produced by GLOW and GOLD LOS code on January 20, 6 UT. The satellite position has been adjusted to 78ºW and 0ºN from the true GOLD position (47.5ºW and 0ºN) such that the satellite is observing the day-time hemisphere given the date and time of the WAM model runs.

Figure 2: LBH spectrum produced from band model (courtesy of Scott Budzien) at 3 temperatures. Each labeled feature corresponds to a vibrational energy transition within the N_2 molecule. The broadening of each feature is due to an increase in occupied rotational levels with increased temperature.

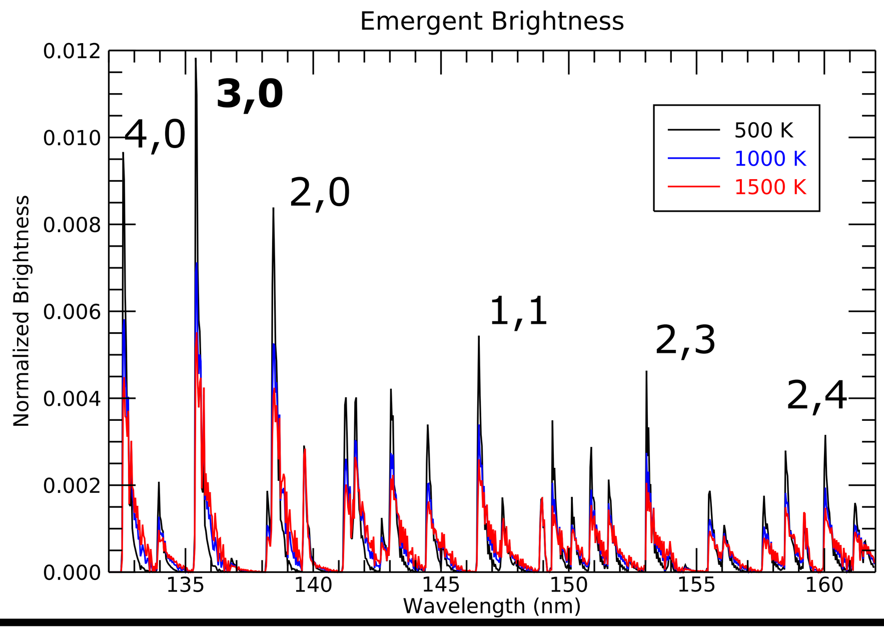

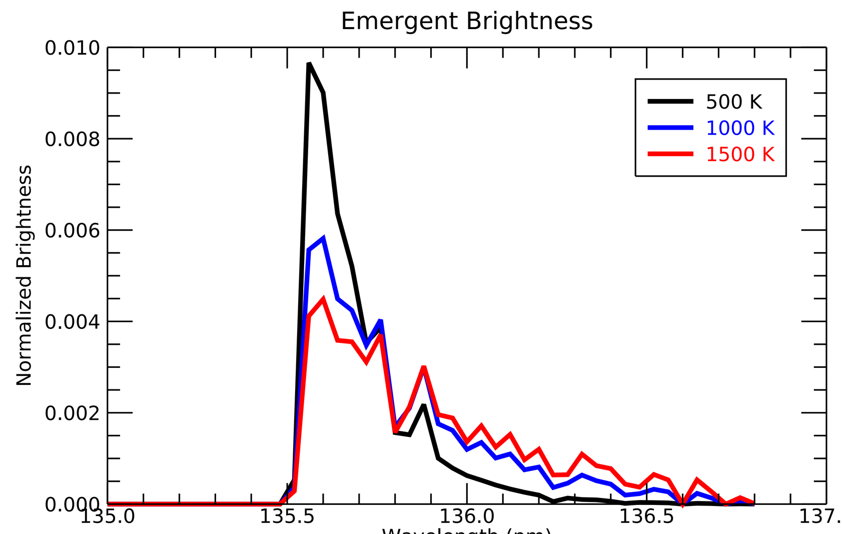

Figure 3: Focusing on the **3,0** transition better illustrates the broadening of the feature to higher wavelengths with increased temperature. This feature, specifically between the wavelengths of 135.5-135.8 nm, is assimilated in the ensemble filter.

Ensemble Filter Approach

Due to the high-dimensionality of the underlying dynamics and non-linearity of LBH emissions with temperature, an ensemble-based data assimilation approach is necessary to make the global temperature profile inference problem tractable. The ensemble square root filter (EnSRF) (Tippett et al., 2003) uses sample statistics based on an ensemble of model forecasts to compute the impact that observations have on the inference of model state variables. The prior covariance of the temperature at each altitude is computed via the equations below. Where *D* is a matrix composed of the mean-subtracted temperature of each model ensemble member, *m*, at each altitude

$$P_{ens} \approx DD^T \quad [1]$$

$$D = \frac{1}{\sqrt{m-1}}[(x^1-\mu)...(x^m-\mu)] \quad [2]$$

In the update step, the prior ensemble (forecast) is deterministically shifted to the posterior (analysis) ensemble, such that the transform $D^a = D^f\mathbf{T}$ is consistent with the Kalman covariance update $\mathbf{P^a} = (\mathbf{I} - \mathbf{KH})\mathbf{P^f}$. Where D^f and D^a are matrices composed of the mean adjusted prior and posterior model ensemble, respectively.

$$\mathbf{P}^a = [\mathbf{I} - \mathbf{P}^f\mathbf{H}^T(\mathbf{R} + \mathbf{H}\mathbf{P}^f\mathbf{H}^T)^{-1}\mathbf{H}]\mathbf{P}^f \quad [3]$$

$$D^a(D^a)^T = D^f[\mathbf{I} - (D^f)^T\mathbf{H}^T(\mathbf{R} + \mathbf{H}D^f(D^f)^T\mathbf{H}^T)^{-1}\mathbf{H}D^f](D^f)^T \quad [4]$$

$$= D^f\mathbf{T}\mathbf{T}^T(D^f)^T$$

In these equations, **H** is the observation operator, $\mathbf{H}D^f$ is a matrix composed of the mean adjusted prior observation ensemble obtained from the GLOW and LOS model outputs, and **R** is the observation error. The transformation matrix **T** is obtained as the square root of the term in brackets in Equation 4. This ensemble-based approximation allows the covariance to track non-linear dynamics with a moderate computational cost (Evenson, 2009).

Information Across LBH Spectrum

Attenuation of LBH emissions is primarily due to O_2 absorption. The equations below describe the radiative transfer model along the GOLD line-of-sight. Given that the O_2 absorption cross section varies over the LBH bandwidth, we investigated the altitude sensitivity of each emission feature to temperature. The results demonstrated a high absolute correlation above 150 km but with minimal difference across the spectrum. As a result, the 3,0 transition was chosen for assimilation due to its relative brightness.

$$I_{LBH} = \frac{1}{4\pi}\int N_{N_2}(z')g_{N_2}(z')e^{-\tau_{O_2}}dz \quad [5]$$

$$g_{N_2} = \int \sigma_{N_2}(E)\Phi(E,z)dE \quad [6]$$

$$\tau_{O_2} = \int N(z')\sigma(T,\lambda)dz \quad [7]$$

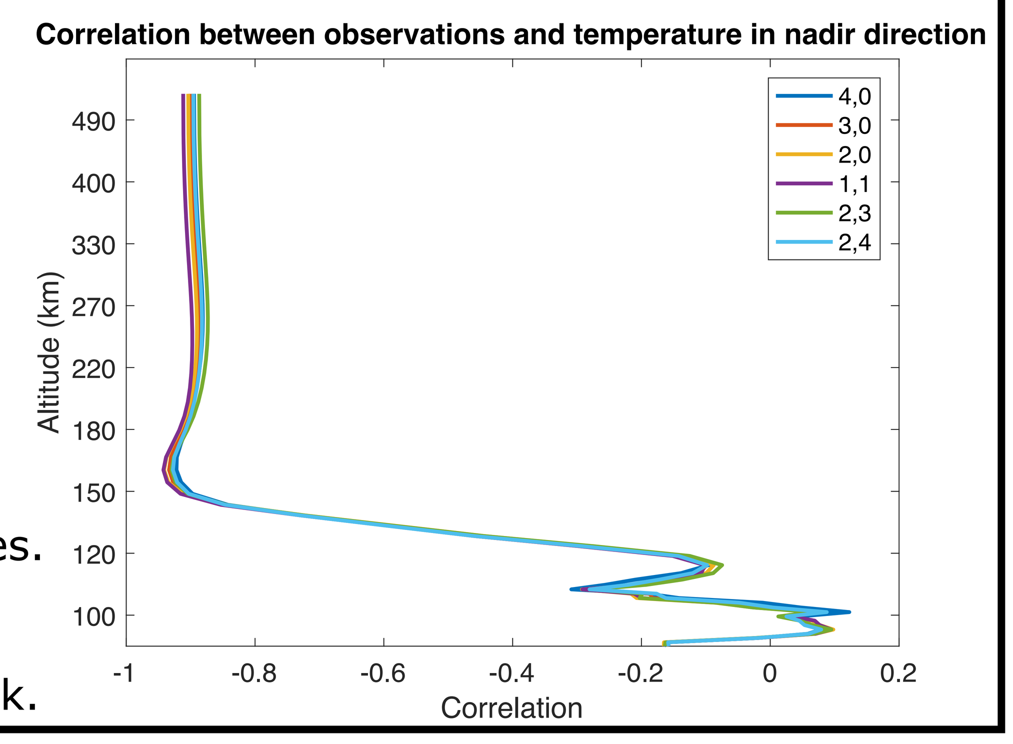

Figure 4: Correlation between observations and temperature at each altitude for the primary emission features shows minimal difference between features. The radiative transfer model does not include the O_2 cross section temperature dependence but will be added in later work.

Ensemble Filter Implementation

Temperature (D^f) NOAA WAM 80 member ensemble → **LBH measurements** (HD^f) NCAR GLOW and radiative transfer model → Compute forecast sample statistics, assimilate "truth" observations and update ensemble statistics

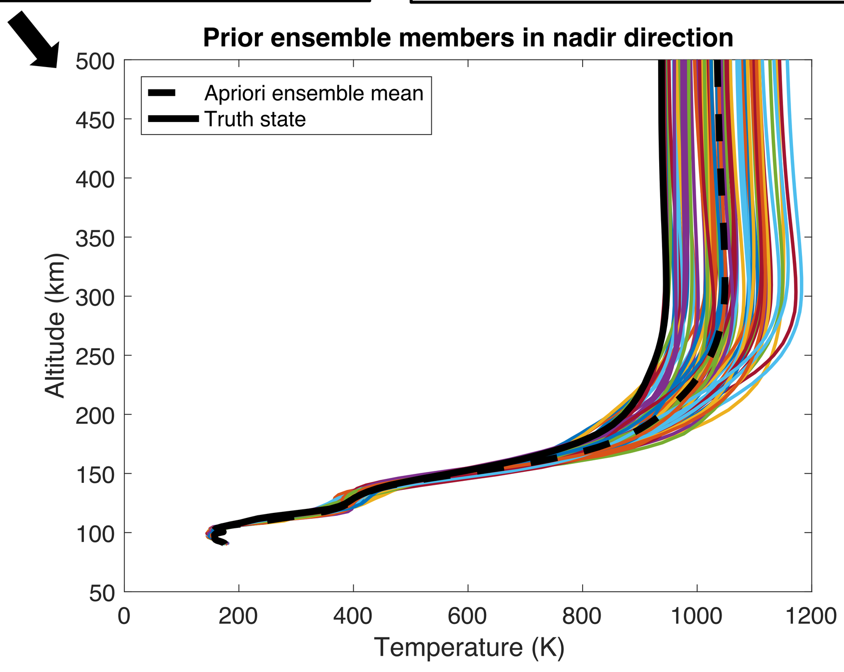

Figure 5: Initial ensemble of temperature profiles. The "truth" state from a nature run is shown in solid black line.

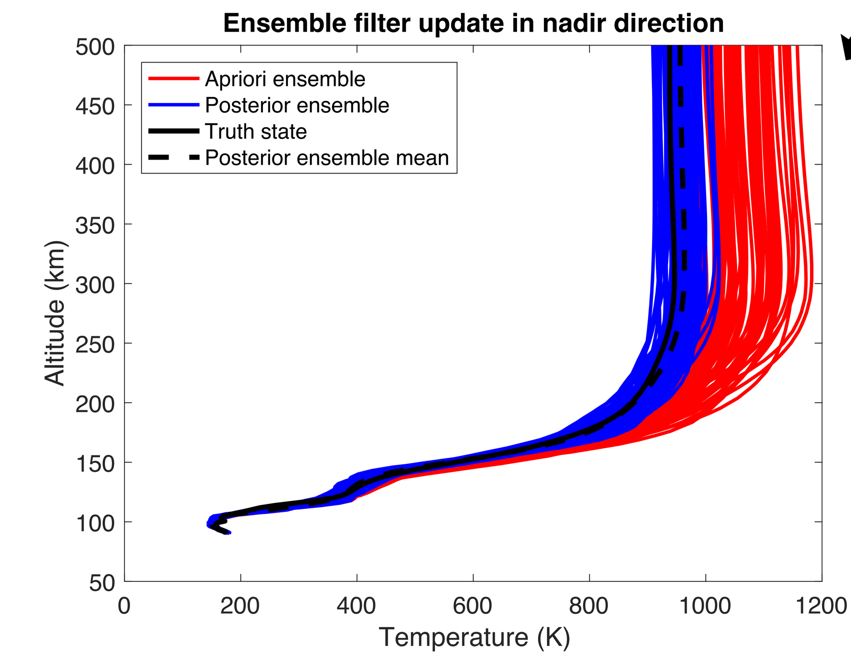

Figure 6: Posterior ensemble (blue) shows assimilation of emission reduced variance and shifted mean closer to truth state.

Results

Figure 8 (Below): Prior and posterior mean temperature error at each altitude over GOLD facing hemisphere. In general, the truth state normalized difference in temperature drops by >10% at altitudes above 200 km over the disk given the ensemble and truth state chosen. The region near the top of disk in the plot with high posterior error corresponds to the edge of the night-time region with low LBH emissions highlighted in the top left corner of **Figure 1**.

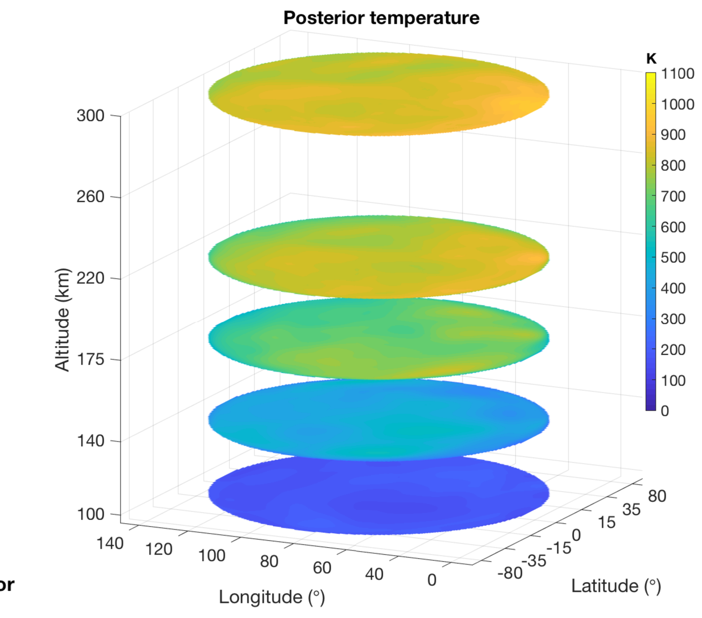

Figure 7 (Above): Inferred (posterior mean) temperature over the disk at 5 altitude levels in the thermosphere.

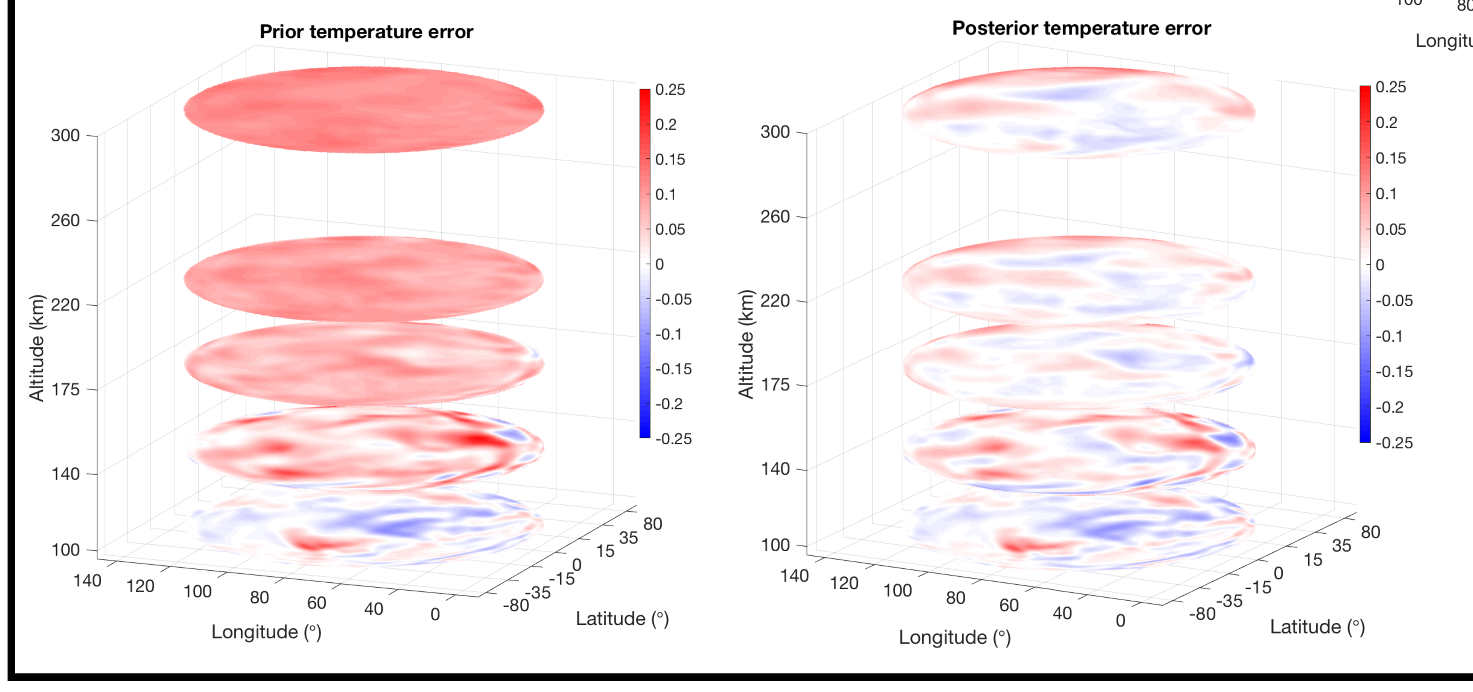

Conclusions and Future Work

The preliminary results of the thermospheric temperature profile inferential problem from GOLD observations using an EnSRF approach demonstrate the sensitivity of the LBH spectrum to altitude-specific temperatures along the line-of-sight. A major missing piece in the current implementation is effects of realistic measurement noises and systematic instrument artifacts. These effects will be important to more accurately specify the observation error, **R**. Moving forward an instrument simulator will be included along with the temperature dependence of the O_2 absorption cross section. Furthermore, because the magnitude of LBH emissions varies with many geophysical factors, the ratio between emissions at shorter wavelengths to those at longer wavelengths within the feature will be assimilated to isolate the temperature-dependent feature profile.

References and Acknowledgments

1. Akmaev, R. A. Rev. Geophys., 49, 2011.
2. Solomon, S. Journal of Geophysical Research - Space Physics, 122, 2017.
3. Aksnes, A. et al. Geophysical Research Letters, 33, 2006.
4. Tippett, M. K., J. L. Anderson, C. H. Bishop, T. M. Hamill, and J. S. Whitraker, Mon. Weather Rev., 131, 1485-1490, 2003.
5. Evenson, G. Data Assimilation: The Ensemble Kalman Filter, Springer Berlin. 2009.

Acknowledgment: We would like to thank Stan Solomon of NCAR for his guidance and support with the GLOW and GOLD LOS models, both critical components of this work.